

Wave fronts, pulses and wave trains in photoexcited superlattices behaving as excitable or oscillatory media

J. I. Arana¹, L. L. Bonilla¹, H. T. Grahn²

¹G. Millán Institute of Fluid Dynamics, Nanoscience and Industrial Mathematics, University Carlos III de Madrid, Av. Universidad 30, 28911 Leganés, Spain

²Paul Drude Institute for Solid State Electronics, Hausvogteiplatz 5–7, 10117 Berlin, Germany

E-mail: joseignacio.arana@uc3m.es

E-mail: bonilla@ing.uc3m.es

E-mail: htgrahn@pdi-berlin.de

Abstract. Undoped and strongly photoexcited semiconductor superlattices with field-dependent recombination behave as excitable or oscillatory media with spatially discrete nonlinear convection and diffusion. Infinitely long, dc-current-biased superlattices behaving as excitable media exhibit wave fronts with increasing or decreasing profiles, whose velocities can be calculated by means of asymptotic methods. These superlattices can also support pulses of the electric field. Pulses moving downstream with the flux of electrons can be constructed from their component wave fronts, whereas pulses advancing upstream do so slowly and experience saltatory motion: they change slowly in long intervals of time separated by fast transitions during which the pulses jump to the previous superlattice period. Photoexcited superlattices can also behave as oscillatory media and exhibit wave trains.

PACS numbers: 73.63.Hs, 05.45.-a, 73.50.Fq, 72.20.Ht

1. Introduction

Vertical nonlinear charge transport in undoped, weakly coupled, photoexcited superlattices (SLs) has many similarities to extended excitable or oscillatory media. In both cases, traveling waves such as wave fronts, pulses, or wave trains play an important role in the dynamics of the system.[1] In undoped SLs, the formation and dynamics of electric field domains (EFDs) are the basic mechanisms behind more complex phenomena such as self-sustained oscillations of the current (SSOC) through voltage-biased SLs, chaos, etc. Interfaces separating EFDs are wave fronts or wave front-bound pulses, and pulses are the building blocks of wave trains. While there are at least two stable EFDs with an almost constant value of the electric field in the case of doped SLs, there may be only one stable EFD in the case of an undoped SL under high photoexcitation.[2] This is similar to what happens in excitable media such as those described by the FitzHugh-Nagumo (FHN) model for nerve conduction.[3, 4] For background information on this model and related models, see Refs. [5, 6, 7, 8, 9, 10, 11, 1]. The case of an oscillatory medium in which there is a single unstable spatially homogeneous state can also be realized in both the FHN model and a strongly photoexcited undoped SL.[2] However, the electric field in a voltage-biased SL with a finite number of periods is constrained to have a fixed area underneath its spatial profile, and this constraint causes it to exhibit a more complex behavior.[2]

The key ingredient to the complex dynamics of electron transport in photoexcited undoped SLs is the introduction of an electron-hole recombination coefficient, which is a function of the electric field. Nonlinear charge transport in weakly coupled undoped type-I superlattices (SL) under photoexcitation is well described by spatially discrete drift-diffusion systems (DDDS) of equations.[12, 13, 14] In earlier models, the electron-hole recombination was considered to be a constant, independent of the electric field.[12] In this case, there are three stable states with spatially homogeneous field profiles, and the predicted nonlinear phenomena are then quite similar to the ones observed in the much better known case of doped SLs (in which the hole density is replaced by a constant doping density): the dynamics is organized by stable wave fronts that join the stable homogeneous states.[14] Introducing a field-dependent electron-hole recombination coefficient in the model has striking consequences.[2] For high photoexcitation densities, it is possible to find only one stable EFD, not two as in the case of a constant recombination coefficient.[12] Then, under a dc voltage bias, periodic or chaotic SSOC may appear. The field profile during self-oscillations may exhibit nucleation of dipole waves inside the sample, splitting of one wave in two, and motion of the resulting waves in opposite directions. Despite the strong asymmetry induced by the drift terms in the equations, these dipole waves resemble the pulses in the FHN model for nerve conduction[9, 11] and are quite different from field profiles for a field-independent recombination coefficient.[12]

In this paper, we construct relevant stable solutions of the DDDS of equations for dc-current-biased SL by means of asymptotic and numerical methods that extend

and refine those used for the discrete FHN system.[15, 16] For an undoped SL that acts as an excitable medium (only one stable EFD), we find that electric field pulses moving downstream with the electron flux can be described using matched asymptotic expansions based on separating the sharp leading and trailing wave fronts of the pulse from smoother regions outside them. Pulses moving upstream do so much more slowly and experience a saltatory motion, in which intervals of a slow change are separated by fast changes during which the pulse jumps to the previous SL period. For an undoped SL acting as an oscillatory medium (a single unstable EFD), we construct periodic wave trains consisting of an infinite succession of pulses.

2. Model equations

Written in nondimensional form, the equations governing nonlinear charge transport in a weakly coupled, undoped, photoexcited GaAs/Al_xGa_{1-x}As SL are:[2]

$$F_i - F_{i-1} = \nu (n_i - p_i) , \quad (1)$$

$$\delta \frac{dF_i}{dt} + n_i v(F_i) - D(F_i)(n_{i+1} - n_i) = J , \quad (2)$$

$$\frac{dp_i}{dt} = 1 - r(F_i) n_i p_i , \quad (3)$$

where i takes on integer values corresponding to the spatial periods of the SL. F_i , n_i and p_i are the average electric field, electron and hole surface densities at the i^{th} SL period, respectively, and the dimensionless parameters ν , δ , and r are described below. Equation (1) refers to the averaged Poisson equation, while Eq. (2) corresponds to Ampère's law: the total current density J equals the sum of the displacement current density $\delta dF_i/dt$ and the electron tunneling current density across the i^{th} barrier that separates wells i and $i + 1$, i.e., $J_{i \rightarrow i+1} = n_i v(F_i) - D(F_i)(n_{i+1} - n_i)$. Note that the tunneling current density has a discrete drift term with electron velocity $v(F)$ and a diffusive term with diffusion coefficient $D(F)$. Charge continuity is obtained by differentiating Eq. (1) with respect to time and using Eq. (2) in the result:

$$\nu \delta \frac{d}{dt}(n_i - p_i) + J_{i \rightarrow i+1} - J_{i-1 \rightarrow i} = 0 . \quad (4)$$

Tunneling of holes is neglected so that only photogeneration and recombination with electrons enter Eq. (3). The field-dependent quantities v , D , and the recombination coefficient r are described in Ref. [2] and their field dependencies are depicted in Fig. 1. The dimensionless parameter ν is a ratio between the carrier density scale determined by photogeneration and recombination and the carrier density determined by scattering processes. The dimensionless parameter δ is the ratio between the time scales of dielectric relaxation and recombination.[2] These parameters depend on the photoexcitation density and the Al content $x \in (0, 1]$ in the SL barriers. For high photoexcitation densities, $\delta \ll 1$, whereas $\delta \gg 1$ for small photoexcitation densities. The parameter ν can be of any order.

It is interesting to depict the phase plane corresponding to spatially uniform solutions of Eqs. (1)–(3) with $n_i = p_i = p$, $F_i = F$:

$$\delta \frac{dF}{dt} = J - p v(F), \quad \text{and} \quad \frac{dp}{dt} = 1 - r(F) p^2. \quad (5)$$

Generically and for fixed J , the nullclines $v(F) p = J$ and $r(F) p^2 = 1$ intersect in one or three fixed points, depending on the Al content x in the barriers, a parameter that controls the functions $v(F)$, $D(F)$ and $r(F)$. [2] At these fixed points,

$$j(F) = J, \quad j(F) = \frac{v(F)}{\sqrt{r(F)}}. \quad (6)$$

The function $j(F)$ is depicted in Fig. 2. For $0.45 \leq x \leq 1$, there are three fixed points of the system in Eq. (5), one on each of the three branches of $p = J/v(F)$, and the

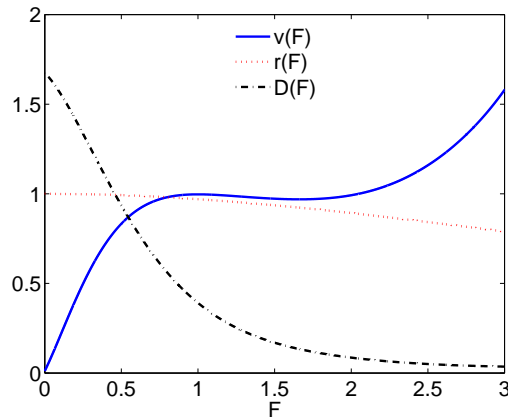


Figure 1. (Color online) Electron velocity v , diffusion coefficient D , and recombination coefficient r vs electric field F for a GaAs/Al_{0.3}Ga_{0.7}As SL with a well width $L_W = 10$ nm and barrier width $L_B = 4$ nm. The lattice temperature is assumed to be 200 K.

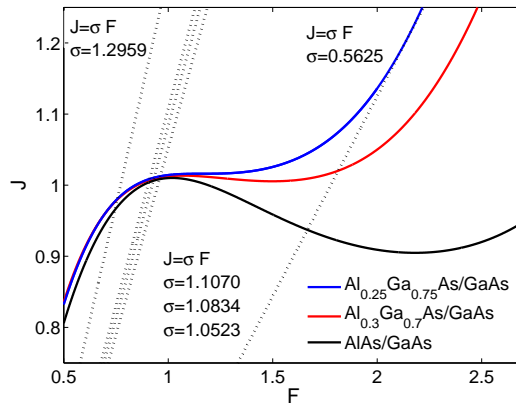


Figure 2. (Color online) Local current density j vs electric field F . For a fixed value of the total current density J , there may be one or three zeros of $j(F) - J$ depending on the Al content x . The dashed lines are the boundary condition $J = \sigma F$ for the different values of the dimensionless contact conductivity σ indicated in the figure.

ratio between $j_{\max} - j_{\min}$ and the average current $(j_{\max} + j_{\min})/2$ is sufficiently large. In this case, nonlinear phenomena are quite similar to those observed in doped SL: static electric field domains with domain walls joining the stable branches of $p = J/v(F)$, SSOC in voltage-biased SL due to the recycling of pulses formed by two moving domain walls bounding a high field region, etc. For $0 < x < 0.45$, $j(F)$ is either increasing for positive F (if $0 < x < 0.25$) or the ratio $2(j_{\max} - j_{\min})/(j_{\max} + j_{\min})$ is small (if $0.25 < x < 0.45$). For $0 < x < 0.25$, there is a unique fixed point at $F = F_*$, which for an appropriate value of J may be located at any of the three branches of $p = J/v(F)$. If the fixed point is located at one of the two stable branches of $p = J/v(F)$ for which $v(F)$ has a positive slope, the dynamical system of Eq. (5) is excitable, whereas it is oscillatory if the fixed point is located on the second branch of $v(F)$ with negative slope. We shall see later that quite unusual phenomena are found for these cases. Under dc current bias, it is possible to have pulses moving to the right or to the left and periodic wave trains. Under dc voltage bias, these pulses and wave trains may give rise to SSOC.[2]

3. Wave fronts in a dc-current-biased photoexcited SL behaving as an excitable medium

Wave fronts and pulses of the electric field and carrier densities are key elements in the description of stable solutions of our model equations. We will start by describing these solutions for an infinite SL under constant current bias J in the limit of high photoexcitation densities, $\delta \ll 1$, in which the dynamical behavior of the SL is richer.[2] In this Section, we focus our attention on wave fronts, while we will deal with pulses in the next Section.

3.1. Leading order construction of wave fronts

A wave front is a moving interface separating regions of smooth field variation on the time scale t . Inside the front, F_i varies rapidly on the time scale t/δ . Let us eliminate the electron density n_i by using Eq. (1) in Eqs. (2)–(3):

$$\begin{aligned} \delta \frac{dF_i}{dt} + v(F_i) \frac{F_i - F_{i-1}}{\nu} - D(F_i) \frac{F_{i+1} + F_{i-1} - 2F_i}{\nu} \\ = J - v(F_i)p_i + D(F_i)(p_{i+1} - p_i), \end{aligned} \quad (7)$$

$$\frac{dp_i}{dt} = 1 - r(F_i)p_i \left(p_i + \frac{F_i - F_{i-1}}{\nu} \right), \quad (8)$$

In the regions where the field varies smoothly, we can set $\delta = 0$, $F_i = F_{i-1}$, $n_i = p_i$ in Eqs. (7)–(8), thereby obtaining the reduced problem

$$p_i v(F_i) = J, \quad (9)$$

$$\frac{dp_i}{dt} = 1 - r(F_i)p_i^2. \quad (10)$$

In the wave fronts that separate these regions, the electric field and the hole density vary rapidly as $F_i(t) = F(\xi)$, $p_i(t) = p(\xi)$, with $\xi = i - ct/\delta$. In these regions, Eqs. (7)

and (8) yield to leading order

$$-c \frac{dF}{d\xi} = J - \left[p + \frac{F(\xi) - F(\xi - 1)}{\nu} \right] v(F(\xi)) + D(F(\xi)) \frac{F(\xi + 1) + F(\xi - 1) - 2F(\xi)}{\nu}, \quad (11)$$

$$-c \frac{dp}{d\xi} = 0. \quad (12)$$

Thus p is a constant equal to the value $p_i(t)$ at the last point in the region of smooth variation before the front. Let $F^{(1)}(p) < F^{(2)}(p) < F^{(3)}(p)$ be the solutions of $J/v(F) = p$ for $v_{\min} < J/p < v_{\max}$, where the local maximum and minimum of the velocity $v(F)$ are reached at (F_{\max}, v_{\max}) and at (F_{\min}, v_{\min}) , respectively (with $F_{\max} < F_{\min}$). Let us assume that the front velocity is positive, $c > 0$. Equation (11) has *decreasing* front solutions (DFs) such that the profile $F(i - ct/\delta)$ is a decreasing function satisfying the boundary conditions:

$$F(-\infty) = F_i(+\infty) = F^{(3)}(p), \quad F(+\infty) = F_i(-\infty) = F^{(1)}(p), \quad (13)$$

and *increasing* front solutions (IFs) with an increasing profile $F(i - ct/\delta)$ that satisfies the boundary conditions:

$$F(-\infty) = F_i(+\infty) = F^{(1)}(p), \quad F(+\infty) = F_i(-\infty) = F^{(3)}(p). \quad (14)$$

In Fig. 3, we show the nullclines $p = J/v(F)$ and $p = [r(F)]^{-1/2}$ for fixed J corresponding to Eq. (5) in a GaAs/AlAs SL. Depending on the parameters, the increasing function $p = [r(F)]^{-1/2}$ may intersect the cubic $p = J/v(F)$ in one, two or three critical points. At least one critical point on the first or third branch of $p = J/v(F)$ makes our system behave as an excitable medium, whereas if there is only one critical point on the second branch of $p = J/v(F)$, our system has an oscillatory character, as we will see later. In Fig. 3, we have also shown a horizontal line for a given constant value of p , which joins the first and third branches of $p = J/v(F)$. This line corresponds to a wave front with fixed p as explained above.

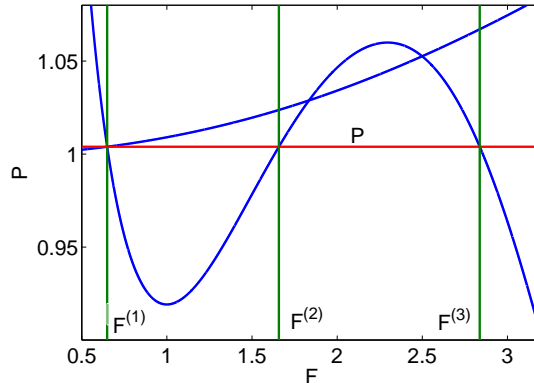


Figure 3. (Color online) p - F phase plane exhibiting nullclines for fixed J and a wave front at constant p in a GaAs/AlAs SL.

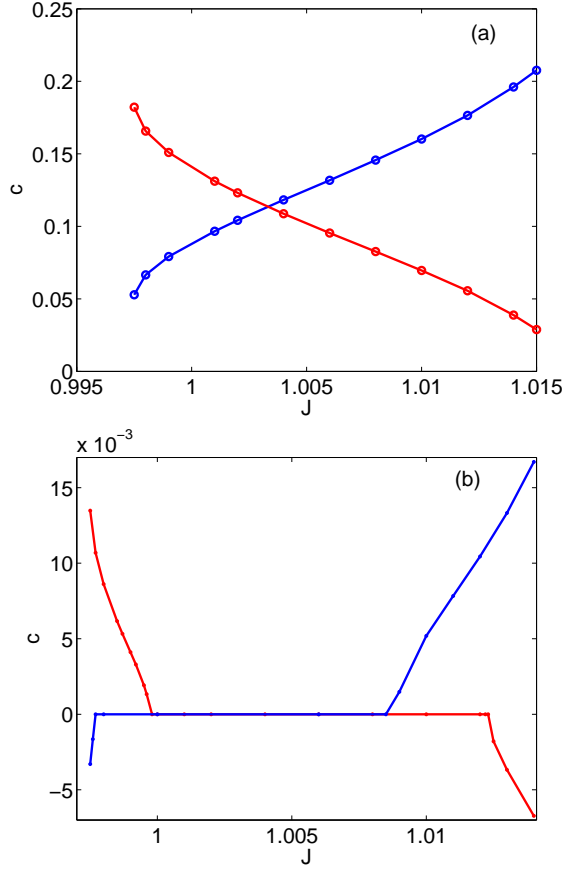


Figure 4. (Color online) Dimensionless velocities of DF and IF as a function of dimensionless current density J for (a) $\nu = 8.45$ and (b) $\nu = 330$ with $x = 0.25$ and p fixed. The DF (resp. IF) velocity increases (resp. decreases) with increasing J .

For sufficiently large ν , there are two critical values of the current density, J_{c1} and J_{c2} , so that IFs move to the right ($c > 0$) if $J < J_{c1}$, are pinned ($c = 0$) if $J_{c1} < J < J_{c2}$, and move to the left ($c < 0$) if $J > J_{c2}$, as shown in Fig. 4(a). A similar picture holds for DFs [cf. Fig. 4(b)]. Near the critical currents J_{ci} ($i = 1, 2$), the wave front profiles and their velocities can be approximately found by means of the theory of active quantum wells (QWs) developed for doped SLs in Ref. [17] (the only change is replacing J/p and ν/p instead of J and ν in the expressions for doped SLs). In the limit $\nu \rightarrow 0+$, the equations for the fronts can be approximated by their continuum limit, which is a first-order hyperbolic partial differential equation having shock waves among its solutions, and the shock velocity gives a good approximation of the wave front velocity.[17]

The theory we have just sketched holds in the limit as $\delta \rightarrow 0$, and we would expect that it also holds for sufficiently small positive values of δ . However, a comparison of the front velocity given by the asymptotic theory with the one obtained by direct numerical simulation shows a remarkable difference even for quite small values of δ . The difference between the approximate and numerical velocities for $\delta = 0.018$ is about 0.06, which gives a relative error of 25%. This error is reduced to 2% for $\delta = 0.001$. Nevertheless, we

would like to have an asymptotic theory, which is better than this. How do we correct the simple wave front construction given above?

3.2. Corrected asymptotic theory of wave fronts

To correct the previous leading order theory of wave fronts, we use the fact that the DF or IF profiles are monotone functions of a variable $\xi = i - ct/\delta$. Thus

$$F_i(t) = \mathcal{F}(\xi), \quad p_i(t) = \mathcal{P}(\xi), \quad (15)$$

with $\mathcal{F}'(\xi) < 0$ (resp. > 0) for DF (resp. IF). In either case, we can find

$$\xi = \Xi(F) \quad \text{which solves} \quad \mathcal{F}(\xi) = F. \quad (16)$$

Then the finite differences

$$\begin{aligned} F_i - F_{i-1} &= \mathcal{F}(\xi) - \mathcal{F}(\xi - 1) = F_i - \mathcal{F}(\Xi(F_i) - 1), \quad \text{and} \\ F_{i+1} + F_{i-1} - 2F_i &= \mathcal{F}(\Xi(F_i) + 1) + \mathcal{F}(\Xi(F_i) - 1) - 2F_i \end{aligned} \quad (17)$$

can be considered to be functions of F_i . Therefore, we can derive from the equation for $p_i(\xi)$

$$-c \frac{dp_i}{d\xi} = \delta \left[1 - r(F_i) p_i \left(p_i + \frac{F_i - F_{i-1}}{\nu} \right) \right] \quad (18)$$

and from the equation for the wave front field profile the following equation for p_i as a function of the field F_i :

$$\frac{dp_i}{dF_i} = \frac{\delta}{J} \frac{1 - r(F_i) p_i \left(p_i + \frac{F_i - F_{i-1}}{\nu} \right)}{1 - \left(p_i + \frac{F_i - F_{i-1}}{\nu} \right) \frac{v(F_i)}{J} + \frac{D(F_i)}{J} \left(p_{i+1} - p_i + \frac{F_{i+1} + F_{i-1} - 2F_i}{\nu} \right)}. \quad (19)$$

Now we integrate this equation and iterate the result starting from the value $p_i(F_0) = p$, thereby obtaining

$$\begin{aligned} p_i &\sim p \\ &+ \frac{\delta}{J} \int_{F_0}^{F_i} \frac{\left[1 - r(F) p \left(p + \frac{F - \mathcal{F}(\Xi(F) - 1)}{\nu} \right) \right] dF}{1 - \left(p + \frac{F - \mathcal{F}(\Xi(F) - 1)}{\nu} \right) \frac{v(F)}{J} + \frac{D(F)}{J} \left(\frac{\mathcal{F}(\Xi(F) + 1) + \mathcal{F}(\Xi(F) - 1) - 2F}{\nu} \right)} \end{aligned} \quad (20)$$

up to terms of order δ^2 .

The starting point F_0 should be selected so as to ensure convergence of the integral in Eq. (20). If $p = p_*$ corresponds exactly to a critical point, we can select F_0 as the field value of the same critical point F_* . Then the integrand has a finite limit as $F \rightarrow F_0$, and the integral in Eq. (20) converges. If this is not the case, we need a nonzero value of the finite difference $F_0 - \mathcal{F}(\Xi(F_0) - 1)$ to obtain a nonzero value of the denominator in Eq. (19). We use the slow scale equation (9) to calculate $F_i = \Phi(p_i)$. Inserting this function in Eq. (10), we obtain

$$\frac{dp_i}{dt} = 1 - r(\Phi(p_i)) p_i^2. \quad (21)$$

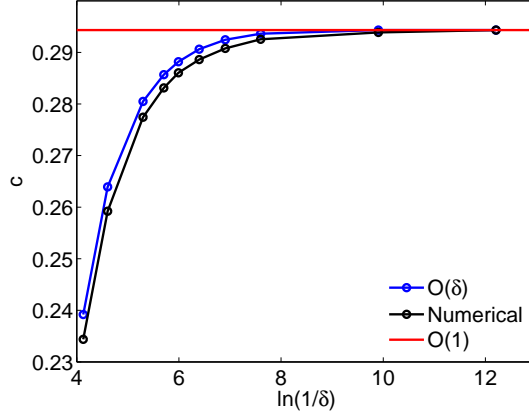


Figure 5. (Color online) Comparison of the numerically obtained and asymptotic approximations for the DF velocity as a function of $\ln(1/\delta)$ using the parameter values $x = 0.3$, $J = 1.006$, and $\nu = 4.449$.

We now solve this equation for an initial value $p_i(0) = p$ to obtain $p_i = p_i(t; p)$. Then $F_i(t) = \Phi(p_i(t; p))$. Using that F_i is a function of $i - ct/\delta$ in the wave front profile, we have $F_{i-1}(t = 0) = F_i(t = -\delta/c) = \Phi(p_i(-\delta/c; p))$. The equation

$$\mathcal{F}(\Xi(F_0) - 1) = \Phi\left(p_i\left(-\frac{\delta}{c}; p\right)\right) \quad (22)$$

determines F_0 as a function of p with $F_0 - \mathcal{F}(\Xi(F_0) - 1) \neq 0$.

Once we have determined p_i as a function of F_i by means of Eq. (20), we can solve the fast equation

$$\begin{aligned} -c \frac{dF_i}{d\xi} + \left(p_i(F_i) + \frac{F_i - F_{i-1}}{\nu}\right) v(F_i) \\ - D(F_i) \left(p_{i+1}(F_{i+1}) - p_i(F_i) + \frac{F_{i+1} + F_{i-1} - 2F_i}{\nu}\right) = J \end{aligned} \quad (23)$$

with $F_i = F(\xi)$, $F_{i\pm 1} = F(\xi \pm 1)$, and boundary conditions (for $c > 0$)

$$F_i(-\infty) = F(+\infty) = F^{(3)}(p'), \quad \text{and} \quad F_i(+\infty) = F(-\infty) = F^{(1)}(p), \quad (24)$$

for the IFs and

$$F_i(-\infty) = F(+\infty) = F^{(1)}(p'), \quad \text{and} \quad F_i(+\infty) = F(-\infty) = F^{(3)}(p), \quad (25)$$

for the DFs. In Eq. (24), the value $p' \neq p$ is determined by solving Eqs. (20) and (23), until the first branch of $J/v(F)$ is reached. Similarly, for a DF, p' in Eq. (25) is found by solving Eqs. (20) and (23), until the third branch of $J/v(F)$ is reached. The front velocity is now a function of δ , and Fig. 5 shows that it is a much better approximation to the numerically calculated front velocity than that given by the leading order theory. In practice, it is easier to calculate directly the finite differences $\mp(F_i - F_{i\pm 1})$ as functions of F_i .

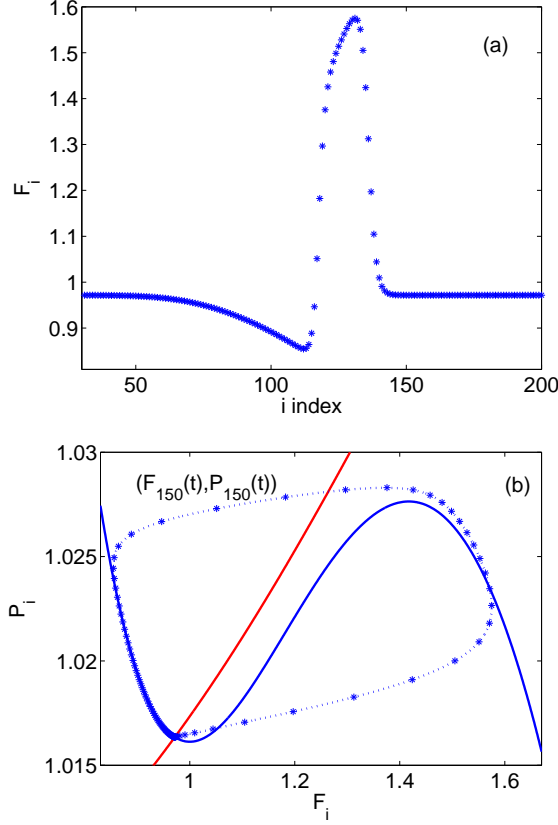


Figure 6. (Color online) (a) Numerically obtained field profile of a pulse moving with positive velocity for $J = 1.013$, $\nu = 8.44565$, $\delta = 3.7288 \times 10^{-3}$. (b) Phase plane showing the nullclines and the motion of the 150th QW as the pulse traverses it. The laser intensity is 120.5 kW/cm^2 .

4. Pulses moving downstream in an excitable SL

As we see in Fig. 6(a), a pulse moving downstream with *positive* velocity consists of regions of smooth field variation on the time scale t , separated by sharp interfaces in which F_i varies rapidly on the time scale t/δ . To find an asymptotic approximation to the pulse profile, we first use the leading order description of its component wave fronts, according to which p_i is a constant independent of i inside the wave front. We can now discuss different regions in the asymptotic description of a pulse, recalling that the field profile is the mirror image of the motion of a QW, $F_i(t) = F(i - ct/\delta)$.

4.1. Only one critical point on a stable branch of $J/v(F)$ (leading order theory)

First of all, we shall describe the pulses for values of J and ν such that there is one critical point (F_*, p_*) located on the first branch of $J/v(F)$. There are no other critical points or, if they exist, they are located on the second branch of $J/v(F)$. Similar results are obtained if the critical point is on the third branch of $J/v(F)$.

- The region of smooth variation of F in front of the pulse is described by Eqs. (9)

and (10). In this region, $F_i = F^{(1)}(p_i)$ so that

$$\frac{dp_i}{dt} = 1 - r(F^{(1)}(p_i)) p_i^2,$$

and initial data evolve exponentially fast toward equilibrium, $F_i = F_*$, $p_i = p_*$.

- For the pulse leading edge, let $p(t)$ be the value of p_i at the last point of the region in front of the pulse. Eventually, $p \rightarrow p_*$. At the leading edge, $F_i(t) = F(i - ct/\delta)$ is a DF moving toward the right with velocity $C = c(J, \nu, p)/\delta$ measured in QWs per unit time t . The DF satisfies Eq. (11) with the boundary conditions in Eq. (13). It is convenient to call $c_-(p) = c(J, \nu, p)$. Eventually, $C \sim c_-(p_*)/\delta$, and F_i decreases from $F_i = F_{\max}$ to $F_i = F_*$ across the leading edge of the pulse.
- For the region between fronts, $F_i = F^{(3)}(p_i)$ and

$$\frac{dp_i}{dt} = 1 - r(F^{(3)}(p_i)) p_i^2.$$

There is a finite number of points in this region. On its far right, $p_i = p \rightarrow p_*$. As we move toward the left, p_i increases until it reaches a certain value $P(t)$ corresponding to that in the trailing wave front.

- For the trailing wave front, $p_i(t) = p(\xi) = P$, and $F_i(t) = F(\xi)$ is an IF satisfying Eq. (11) with the boundary conditions of Eq. (14). This front moves with velocity $C = c(J, \nu, P)/\delta$ measured in QWs per unit time t . It is convenient to denote $c_+(P) = c(J, \nu, P)$. We shall indicate how to determine P below. Clearly, if the pulse moves rigidly, we should have $c_+(P) = c_-(p_*)$ after a sufficiently long transient period.
- For the pulse tail, we again have $F_i = F^{(1)}(p_i)$ and $dp_i/dt = 1 - r(F^{(1)}(p_i)) p_i^2$. Sufficiently far to the left, $p_i = p_*$, $F_i = F_*$.

The number of QWs between wave fronts of the pulse can be calculated as follows.[16] Let τ be the delay between fronts, i.e. the time elapsed from the moment, at which the leading front traverses the QW $i = I$, to the moment, when the trailing front is at $i = I$. Clearly,

$$\tau = \int_{p(t-\tau)}^{P(t)} \frac{dp}{1 - r(F^{(3)}(p)) p^2}. \quad (26)$$

The number of QWs between fronts, $m(t)$, is

$$m = \frac{1}{\delta} \int_{t-\tau}^t c_-(p(t)) dt. \quad (27)$$

However, the separation between fronts satisfies the equation

$$\frac{dm}{dt} = \frac{c_-(p(t)) - c_+(P(t))}{\delta}. \quad (28)$$

The three Eqs. (26), (27), and (28) can be solved to obtain the three unknowns τ , m and $P(t)$. The function $p(t)$ is determined by solving Eq. (10) with $F_i = F^{(1)}(p_i)$ in the region to the left of the leading front.

After a transient period, $p(t) \rightarrow p_*$ and $P(t) \rightarrow P$ (a constant value) so that we arrive at the simpler expressions

$$\tau = \int_{p_*}^P \frac{dp}{1 - r(F^{(3)}(p)) p^2}, \quad \text{and} \quad (29)$$

$$\frac{dm}{dt} = \frac{c_-(p_*) - c_+(P)}{\delta} \quad (30)$$

instead of Eqs. (26) and (28), respectively. The number of points at the pulse top is now

$$m = \frac{c_-(p_*)\tau}{\delta} = \frac{c_-(p_*)}{\delta} \int_{p_*}^P \frac{dp}{1 - r(F^{(3)}(p)) p^2}. \quad (31)$$

This equation yields P as a function of m . Then Eq. (30) becomes an autonomous differential equation for m that has a stable constant solution at $m = m^*$ such that $c_-(p_*) = c_+(P(m^*))$: At $m = m^*$, the right hand side of Eq. (30) has a slope $-[1 - r(F^{(3)}(J/P)) P^2] c'_+(P)/c_-(p_*) < 0$.

Recapitulating, for appropriate initial conditions, leading and trailing fronts of a pulse evolve until m reaches its stable value at which $c_-(p_*) = c_+(P(m^*))$ and Eq. (31) holds. To compute m^* , we first determine $P^* = P(m^*)$ by using $c_-(p_*) = c_+(P(m^*))$. Then we calculate $\tau = \tau^*$ (which does not depend on δ !) from Eq. (29) and $m^* = c_-(p_*)\tau^*/\delta$. Our construction breaks down if the number of QWs between fronts falls below 1. This yields an upper bound for the critical value of δ above which pulse propagation fails: $\delta_c \sim c_-(p_*)\tau^*$. Pulse propagation may also fail if the leading front becomes pinned for a current density on the interval (J_{c1}, J_{c2}) as mentioned in the previous Section.[1, 17, 18, 19]

To calculate the asymptotic length of the pulse tail, we cannot use Eq. (29) with $F^{(1)}$ replacing $F^{(3)}$ in that formula, because the resulting time becomes infinite. However, we can calculate the time it takes for a solution $p(t)$ of Eq. (21) with $\Phi(p) = F^{(1)}(p)$ and $p(0) = P$ to reach a neighborhood of p_* . From that equation, we obtain

$$t = \int_p^P \frac{dp}{r(F^{(1)}(p))p^2 - 1} \sim \int_{p_*}^P \left[\frac{1}{r(F^{(1)}(p))p^2 - 1} - \frac{1}{(rp^2)'_*(p - p_*)} \right] dp + \frac{1}{(rp^2)'_*} \ln \left(\frac{P - p_*}{p - p_*} \right),$$

with $(rp^2)'_* = d[r(F^{(1)}(p))p^2]/dp|_{p=p_*} > 0$, and therefore

$$p(t) - p_* \sim (P - p_*) e^{-(rp^2)'_*(t-T)}, \quad T = \int_{p_*}^P \left[\frac{1}{r(F^{(1)}(p))p^2 - 1} - \frac{1}{(rp^2)'_*(p - p_*)} \right] dp \quad (32)$$

for long times such that $p(t)$ is sufficiently close to p_* . The time needed for $p(t)$ to go from P to $p_* + (P - p_*)/e$ is then $T_* = T + 1/(rp^2)'_*$. The tail length is approximately given by $M = c_-(p_*)T_*/\delta$.

4.2. Only one critical point on a stable branch of $J/v(F)$ (corrected theory)

How do we correct this pulse construction using our improved theory of wave fronts?

- The region of smooth variation in front of the pulse is as described above.

- However, we have to use Eq. (23) instead of Eq. (11) including the boundary conditions of Eq. (24) or (25) to construct the leading and trailing wave fronts of the pulse. Let us assume that the pulse moves from left to right. The leading wave front is a DF moving with velocity $c_-(p)/\delta$ with $c_-(p) = c(J, \nu, p, \delta)$ given by Eq. (23) and the boundary conditions of Eq. (25). While $p(t)$ is the value at the initial field on the first branch of $J/v(F)$, $p'(t)$ is the hole density at the final QW of the DF which is on the third branch of $J/v(F)$. The time it takes for a QW to move from $(F^{(1)}(p), p)$ to $(F^{(3)}(p'), p')$ is of order δ , and it needs to be considered when constructing the pulse.
- In the region between leading and trailing fronts, $F_i = F^{(3)}(p_i)$. On its far right, $p_i = p' \rightarrow p'_*$, where we call p'_* the value of p' corresponding to $p = p_*$. As we move toward the left, p_i increases until it reaches a certain value $P(t)$ corresponding to that in the trailing wave front.
- The trailing wave front is an IF moving with velocity $c_+(P)/\delta$, with $c_+(P) = c(J, \nu, P, \delta)$ given by Eq. (23) and the boundary conditions of Eq. (24). The hole densities at the initial and final QWs of the IF are P and P' , respectively. The corresponding fields are $F^{(3)}(P)$ and $F^{(1)}(P')$, respectively. Again the time it takes for a QW to move from $(F^{(3)}(P), P)$ to $(F^{(1)}(P'), P')$ is of order δ and will be included in our calculations to order δ .
- The pulse tail is as described above except that its first QW has a hole density P' instead of P .

Equations (26) to (28) become

$$\tau = \int_{p'(t-\tau)}^{P(t)} \frac{dp}{1 - r(F^{(3)}(p)) p^2}, \quad (33)$$

$$m = \frac{1}{\delta} \int_{t-\tau}^t c_-(p(t)) dt, \quad (34)$$

$$\frac{dm}{dt} = \frac{c_-(p'(t)) - c_+(P(t))}{\delta}. \quad (35)$$

After the transient period, these equations become Eqs. (29)–(31) with p' (now time-independent) instead of p_* . The rest of the considerations made above apply except that now τ^* depends on δ because p'_* does.

4.3. Two critical points on the stable branches of $J/v(F)$

In the case illustrated in Fig. 7, there is one critical point on each of the three branches of $J/v(F)$. Let (F_*, p_*) and (F^*, p^*) be the critical points on the first and third branches of $J/v(F)$, respectively. This case is very similar to that described before for the case of a sole critical point on the first branch. However, now $c_-(p_*) \neq c_+(p^*)$ except for particular values of J . Therefore, these pulses do not move rigidly in general: they will shrink and disappear or grow indefinitely. Regions 1 to 3 of the pulse in Fig. 7(a) are identical to those of the pulse with only one critical point, except that now $p \rightarrow p_*$ and $P \rightarrow p^*$, and m either decays to zero or it grows indefinitely.

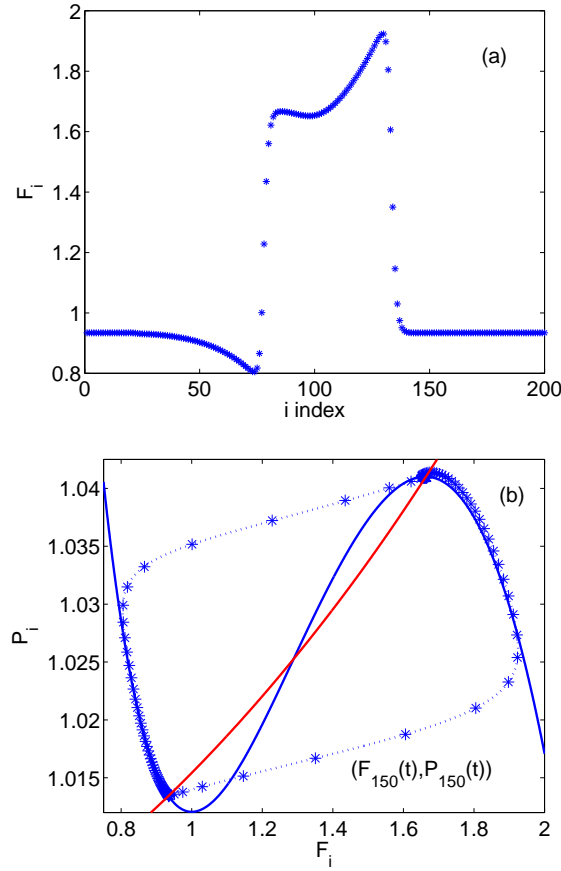


Figure 7. (Color online) (a) Numerically obtained field profile of a pulse moving with positive velocity when there are three critical points in the phase plane. (b) Phase plane showing the nullclines and the motion of the 150th QW as the pulse traverses it. $J = 1.009$. The photoexcitation intensity is 120.5 kW/cm^2 .

5. Wave trains moving downstream in a dc-current-biased photoexcited SL

For the spatially discrete FHN system, wave trains were constructed by A. Carpio using matched asymptotic expansions.[15] A similar construction could be carried out using our improved theory of wave fronts. A wave train consists of a periodic profile $F(\xi)$, $p(\xi)$, $\xi = i - ct/\delta$, with period L and velocity c . Figure 8(a) gives the corresponding field profile: a first smaller pulse triggers a periodic succession of equal pulses, which become the wave train. Figure 8(b) shows the passage of a wave train through a QW: starting at an unstable stationary state, trajectories in the phase plane evolve toward a stable limit cycle. The wave train profiles can be reconstructed from a time periodic solution $F_i(t) = F(i - ct/\delta)$, $p_i(t) = p(i - ct/\delta)$, with time period $T = L\delta/c$ and velocity c . The spatial structure of the wave train at each fixed time t is given by $F_i(t) = F(i - ct/\delta)$ and $p_i(t) = p(i - ct/\delta)$. The points contained in a period satisfy $0 \leq i - ct/\delta \leq L$, that is, $ct/\delta \leq i \leq L + ct/\delta$. As time grows, the discrete points *travel* along the continuous wave profile and are transferred from one period to the next. The number of integers i

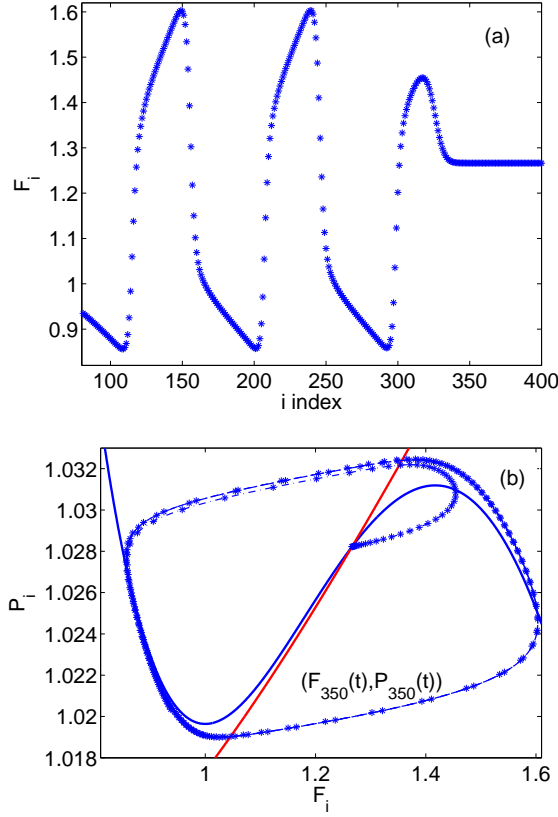


Figure 8. (Color online) (a) Numerically obtained field profile of a pulse moving with positive velocity followed by a wave train when there is only one critical point in the phase plane. (b) Phase plane showing the nullclines and the motion of the 350th QW as the pulse traverses it for $J = 1.0165$. The photoexcitation intensity corresponds to 120.5 kW/cm^2 .

one can fit in an interval of length L is the integer part of L .

Assuming a positive velocity, there are four stages in one time period of the wave trains $(F_i(T, \delta), p_i(T, \delta))$:

- For leading-edge DFs given by Eqs. (20) and (23) using the boundary conditions of Eq. (25), the DF velocity is $c_-(p)/\delta$ with $c_-(p) = c(J, \nu, p, \delta)$, where $p(t)$ is the value at the initial field on the first branch of $J/v(F)$ and $p'(t)$ is the hole density at the final QW of the DF, whose corresponding field is on the third branch of $J/v(F)$. The time it takes for a QW to move from $(F^{(1)}(p), p)$ to $(F^{(3)}(p'), p')$ is of order δ , and we should consider it when constructing the train.
- In the peak region between leading and trailing fronts, $F_i = F^{(3)}(p_i)$. On its far right, $p_i = p'$. As we move toward the left, p_i increases until it reaches a certain value $P(t)$ corresponding to that in the trailing wave front. $P(t)$ will be calculated later. The duration of this stage is

$$T_p = \int_{p'}^P \frac{dp}{1 - r(F^{(3)}(p)) p^2}. \quad (36)$$

Note that T_p may become infinite if there is a fixed point (F^*, p^*) on the third branch of $J/v(F)$. In such a case, we may have wave trains only if $p < p^*$.

- The trailing wave front is an IF moving with velocity $c_+(P)/\delta$, with $c_+(P) = c(J, \nu, P, \delta)$ given by Eq. (22) and the boundary conditions of Eq. (24). The hole densities at the initial and final QWs of the IF are P and P' , respectively, and the corresponding fields are $F^{(3)}(P)$ and $F^{(1)}(P')$, respectively. Again the time it takes for a QW to move from $(F^{(3)}(P), P)$ to $(F^{(1)}(P'), P')$ is of order δ and will be ignored. For the wave train to move rigidly, we must have $c_-(p) = c_+(P) = c$. This condition gives P as a function of p .

- In the tail of the wave train, $F_i = F^{(1)}(p_i)$. On the far right of the tail region, $p_i = P'$ and p_i decreases until it reaches the value p . The duration of this stage is

$$T_t = \int_{P'}^p \frac{dp}{1 - r(F^{(1)}(p)) p^2}. \quad (37)$$

Note that T_t may become infinite if there is a fixed point (F_*, p_*) on the first branch of $J/v(F)$. In such a case, we may have wave trains only if $p > p_*$.

The previous construction of the wave train gives its velocity and period $T \sim T_p + T_t$ as functions of the parameter p . The spatial period L is the integer part of cT/δ . The number of QWs in the peak (resp. the tail) region is the integer part of $c_-(p)T_p/\delta$ (resp. $c_-(p)T_t/\delta$). Our construction clearly fails if the number of QWs in the peak region is smaller than one, i.e., if $c_-(p)T_p < \delta$. Thus, δ has to be larger than $c_-(p)T_p$.

6. Pulses moving upstream in a dc-current-biased photoexcited SL that behaves as an excitable medium

Numerical simulations of the complete model show pulses moving upstream with a negative velocity, both under dc current bias and under dc voltage bias. Although the field profile of these pulses is quite similar to that of downstream moving pulses (cf. Figs. 6 and 9), there are fundamental differences between them. The velocity of these pulses is much smaller than that of downstream moving pulses, and they cannot be approximated by one IF and one DF plus regions of slow variation of the electric field. In fact, Fig. 4(b) shows that, contrary to the case of wave fronts moving with positive velocity depicted in Fig. 4(a), it is not possible for a DF and an IF to move with the same negative velocity at a fixed J . Thus, our construction of pulses in Section 4 cannot describe pulses that move rigidly upstream with negative velocity.

The asymptotic construction of pulses moving rigidly with negative velocity under dc current bias is necessarily different from the case of downstream moving pulses. The rigid upstream motion of pulses is saltatory: although the velocity of the pulse is constant ($c < 0$), there are periods in which the QWs move slowly on the pulse field profile separated by fast transitions as shown in Fig. 9(a). Figure 9(b) shows that the hole density changes smoothly even at the fast transitions in the field profile. During the slow periods, the field and hole density at the QWs evolve according to the following

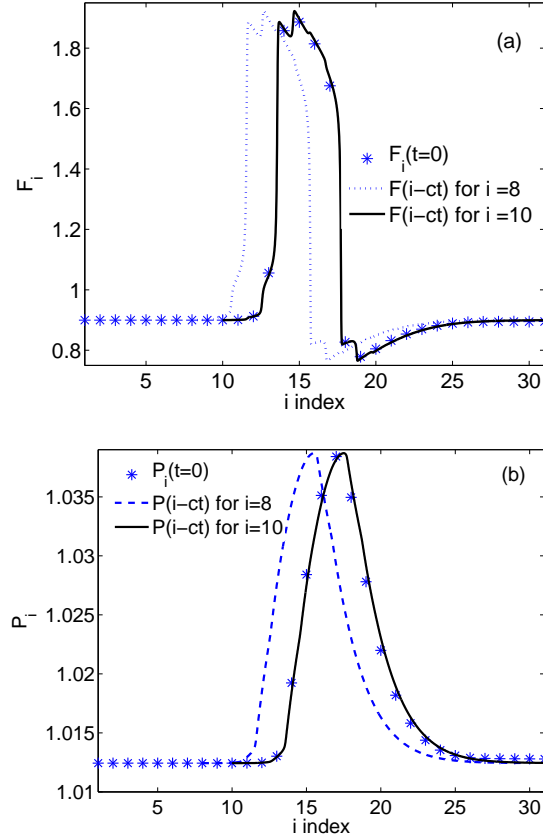


Figure 9. (Color online) (a) Numerically obtained field profile of a pulse moving with negative velocity for $J = 1.009$, $\nu = 70.5$, $\delta = 4.05 \times 10^{-4}$. (b) Numerically obtained hole density profile of the same pulse. The laser intensity is 479.7 kW/cm^2 .

equations:

$$\left(p_i + \frac{F_i - F_{i-1}}{\nu} \right) v(F_i) - \left(p_{i+1} - p_i + \frac{F_{i+1} + F_{i-1} - 2F_i}{\nu} \right) D(F_i) = J, \quad (38)$$

$$\frac{dp_i}{dt} = 1 - r(F_i) p_i \left(p_i + \frac{F_i - F_{i-1}}{\nu} \right), \quad (39)$$

which have been obtained by setting $\delta = 0$ in Eqs. (7)–(8). We have to solve Eq. (38) for the profile $\{F_i\}$ in terms of the instantaneous values of the $\{p_i\}$ and insert the result in Eq. (39). It turns out that there are several possible solutions corresponding to integer shifts of the pulse profile $i \rightarrow i + m$, $m = 0, \pm 1, \dots$. The implicit function theorem establishes that, starting from an appropriate pulse-like initial condition, it is possible to find $F_i = F_i(\{p_j\})$, provided the Jacobian determinant corresponding to Eq. (38) is not zero. This condition holds until the QWs reach the points of abrupt field change in Figs. 9(a) or 10(a) (phase plane) at times $t = t_a$. Then the Jacobian vanishes, and the field values change according to

$$\frac{dF_i}{d\tau} = J + \left(p_{i+1} - p_i + \frac{F_{i+1} + F_{i-1} - 2F_i}{\nu} \right) D(F_i)$$

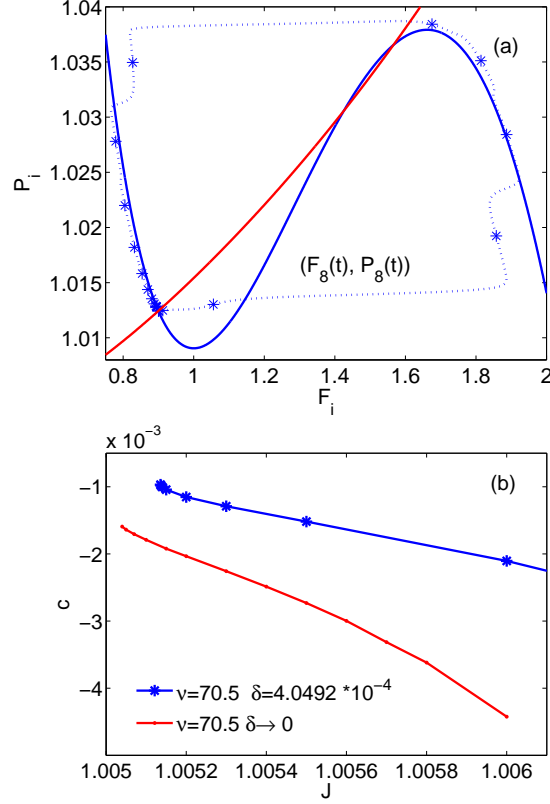


Figure 10. (Color online) (a) Phase plane showing the nullclines and the motion of the 8th QW as the pulse traverses it for the profiles depicted in Fig. 9. (b) Comparison of the pulse velocity obtained from leading order perturbation theory and that obtained from numerical simulations.

$$-\left(p_i + \frac{F_i - F_{i-1}}{\nu}\right) v(F_i), \quad (40)$$

with $\tau = (t - t_a)/\delta$ and $\{p_i\}$ frozen at their values at t_a given by Eqs. (38)–(39). As explained before, as $\tau \rightarrow -\infty$ the $\{F_i(\tau)\}$ tends to the solution of Eq. (38) for $t = t_a$, and it tends to the same profile shifted one step to the left: $i \rightarrow i - 1$ as $\tau \rightarrow +\infty$. Then another slow stage follows. Figure 10(b) shows the velocity of the pulse. It is approximately the inverse time one QW spends in the short interval of p between the abrupt long jump in F from the first branch of $J/v(F)$ to a value below that in the third branch of $J/v(F)$ and the abrupt short jump in F to the third branch of $J/v(F)$, which occurs for a somewhat higher value of p as shown in Fig. 10(a).

Figures 11(a) and 11(b) compare the field and hole density profiles of the reconstructed pulse (moving with positive velocity) and those obtained by direct numerical solution of the equations. Similarly, Figures 12(a) and 12(b) compare the field and hole density profiles of the reconstructed pulse (moving with negative velocity) and those obtained by direct numerical solution of the equations. The agreement is quite reasonable and it could be improved by finding a corrected theory of the pulse velocity.

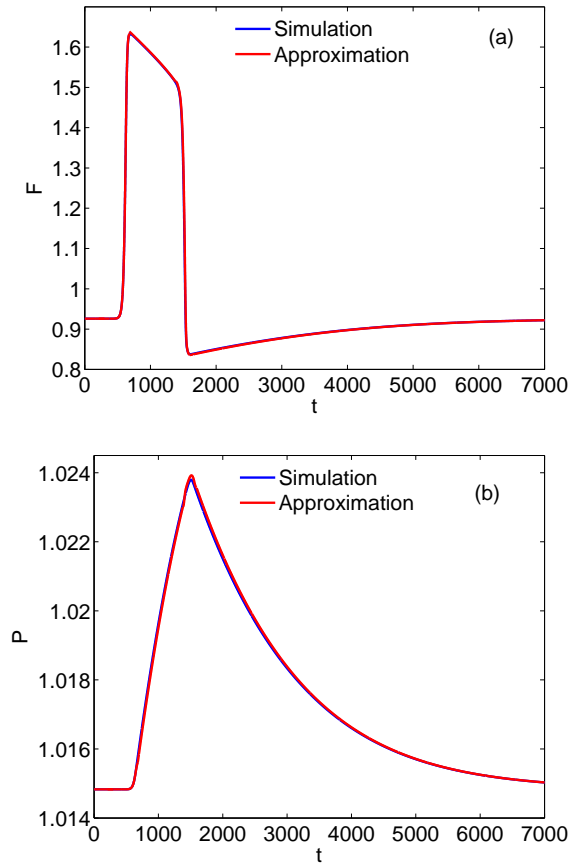


Figure 11. (Color online) (a) Reconstruction of a pulse of the electric field moving with a positive velocity for $J = 1.009$, $\nu = 70.5$, $\delta = 4.05 \times 10^{-4}$ as in Fig. 7. (b) Reconstruction of the corresponding hole density profile.

7. Conclusions

An undoped, strongly photoexcited, weakly coupled, dc-current-biased SL exhibits a variety of pulse and wave front solutions. They can be constructed using matched asymptotic expansions that exploit the large separation of time scales (measured by the dimensionless parameter δ) between the carrier dynamics and the evolution of the electric field. On the time scale of the electron and hole densities, the field follows adiabatically the profiles thereof.

For large photoexcitation, the field profile of a pulse typically consists of slowly varying regions separated by sharp wave fronts. As in the case of the FitzHugh-Nagumo model of nerve conduction, an asymptotic reconstruction of the downstream-moving pulse to leading order in δ determines its velocity as the value for which the velocities of the leading and trailing fronts are the same. The comparison of this approximate velocity to that obtained by direct solution of the full model equations is only fair. For a better agreement, we have improved the description of the wave fronts comprising the pulse by including order δ corrections. The resulting corrected theory describes

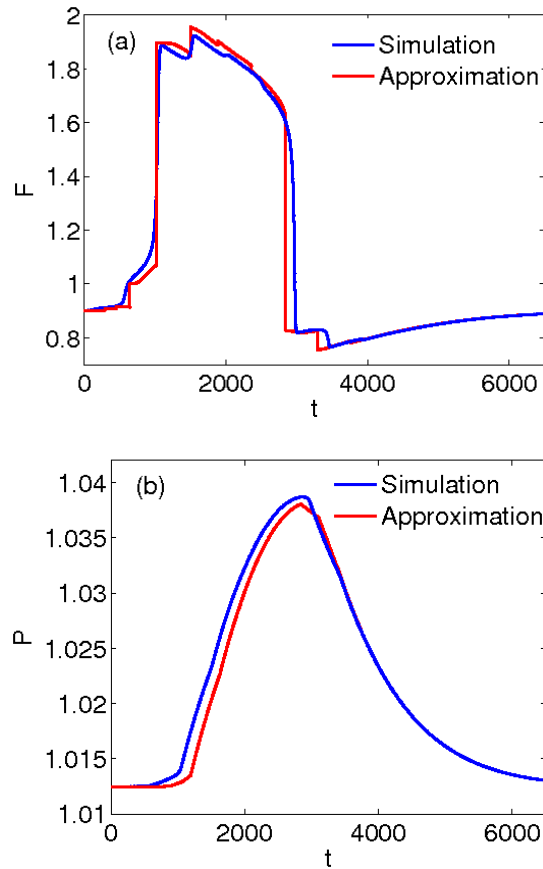


Figure 12. (Color online) (a) Reconstruction of a pulse of the electric field moving with a negative velocity for $J = 1.009$, $\nu = 70.5$, $\delta = 4.05 \times 10^{-4}$. (b) Reconstruction of the corresponding hole density profile.

the pulses and their velocities much better. Pulses moving upstream the electron flow exhibit saltatory motion: they alternate periods of very small velocity with fast motion during short time intervals. We have reconstructed them using matched asymptotic expansions in the limit of small δ , but the resulting theory is quite different from that of downstream-moving pulses.

Acknowledgments

The work was financially supported in part by the Spanish Ministry of Science and Innovation under grant FIS2008-04921-C02-01.

References

- [1] Bonilla L L, Teitworth S W 2010 *Nonlinear wave methods for charge transport* (Weinheim: Wiley)
- [2] Arana J I, Bonilla L L, Grahn H T 2010 *Phys. Rev. B* **81** 035322.
- [3] FitzHugh R 1961 *Biophys. J.* **1**, 445
- [4] Nagumo J, Arimoto S, Yoshizawa S 1962 *Proc. Inst. Radio Engineers* **50** 2061

- [5] Scott A C 1975 *Rev. Mod. Phys.* **47** 487
- [6] Bell J, Costner C 1984 *Quart. Appl. Math.* **42** 1
- [7] Neu J C, Preissig R S, Krassowska W 1997 *Physica D* **102** 285
- [8] Struijk J J 1997 *Biophys. J.* **72** 2457
- [9] Keener J P, Sneyd J 1998 *Mathematical Physiology* (New York: Springer)
- [10] McIntyre C C, Grill W M 1999 *Biophys. J.* **76** 878
- [11] Murray J D 2001 *Mathematical Biology I. An Introduction*, 3rd ed. (Berlin: Springer)
- [12] Bonilla L L, Galán J, Cuesta J A, Martínez F C, Molera J M 1994 *Phys. Rev. B* **50** 8644
- [13] Bonilla L L 1995 in p. 1 of *Nonlinear Dynamics and Pattern Formation in Semiconductors and Devices*, Springer Proceedings in Physics 79, edited by F.-J. Niedernostheide (Berlin: Springer)
- [14] Bonilla L L, Grahn H T 2005 *Rep. Prog. Phys.* **68** 577
- [15] Carpio A 2005 *Physica D* **207** 117
- [16] A. Carpio A, L.L. Bonilla L L 2003 *SIAM J. Appl. Math.* **63** 619
- [17] Carpio A, Bonilla L L, Dell'Acqua G 2001 *Phys. Rev. E* **64**, 036204
- [18] Carpio A, Bonilla L L 2003 *Phys. Rev. Lett.* **90**, 135502
- [19] Wang J, Zheng G-Z 2008 *Chinese Phys. B* **17** 4129